Article

Rheological Behavior and Filtration of Water-Based Drilling Fluids Containing Graphene Oxide: Experimental Measurement, Mechanistic Understanding, and Modeling

Ali Rafieefar, Farhad Sharif,* Abdolnabi Hashemi, and Ali Mohammad Bazargan

Read Online

ACCESS | Metrics & More | Article Recommendations

ABSTRACT: Any improvement in drilling technology is critical for developing the oil and gas industry. The success of drilling operations largely depends on drilling fluid characteristics. Drilling fluids require enough viscosity to suspend the particles and transport them to the surface and enough capability to control the fluid loss into the formation. Rheology and filtration characteristics of drilling fluids are crucial factors to consider while ensuring the effectiveness of a drilling operation. Graphene oxide (GO), xanthan gum (XG), and low-viscosity carboxymethyl cellulose (CMC LV) are being utilized in this research to produce high-performance, low-solid water-based drilling fluids (WDFs). Rheological and filtration behaviors of GO/XG/CMC LV-WDF were investigated as a function of GO, XG, and CMC LV at low concentrations (0.0−0.3% w/w) and atmospheric conditions. According to the findings, GO improved the rheological and filtration capabilities of the WDF. By adding 0.15 wt % GO, shear stress could be doubled, especially at a high shear rate of 1022 s^{-1}. The plastic viscosity of the fluid could be expanded from 6 to 13 centipoise, and a fluid loss of 8.7 mL over 30 min was observed during the API fluid test, which would be lower than the suggested fluid loss value (15.0 mL) for water-based mud. At the same concentration of XG and CMC LV, XG had a more significant influence on rheological characteristics in the presence of GO. Adding 0.3 wt % XG could increase fluid shear stress from 20.21 to 30.21 Pa at a high shear rate of 1022 s^{-1}. In contrast, CMC LV had more impact on filtration properties, acting as a filtration control agent by decreasing the API fluid loss of fluid from 21.4 to 14.2 mL over 30 min. The addition of XG and CMC LV to the GO solution may influence the microstructure of the filter cake, resulting in a tree-root morphology. Indeed, in the GO/CMC LV solution, the individual platelets may bind together, form a jellyfish shape, and block the micropores. The incorporation of CMC LV helped develop compact filter cakes, resulting in excellent filtration. Five rheological models were employed to match the fluid parameters quantitatively. The Herschel−Bulkley model outperformed the other models in simulating fluid rheological behavior. The findings of this study can be utilize to provide low-cost, stable, and environmentally compatible additives for drilling low-pressure, depleted, and fractured oil and gas reservoirs.
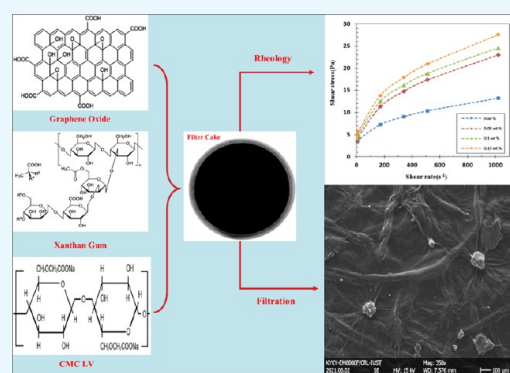
1. INTRODUCTION

The oil and gas industry has taken full advantage of the improvements in drilling technology. Pumping drilling mud into the borehole and then conveying cuttings out of it are essential for the success of drilling operations. Drilling fluids require enough viscosity to suspend the particles and transport them even at low shear rates.[1] It is worth noting that well-designed drilling mud can save the total cost of operation by 5−15%.[2] Drilling muds are divided into three categories such as water-based, synthetic, and oil-based mud. Water-based mud is a more suitable and appealing choice for drilling than synthetic and oil-based mud due to the environmental concerns and costs.[3] These drilling fluids are extensively utilized because they are less expensive and easier to prepare than other types. Water, viscosifiers, filtration control agents, and weighing materials are often used. Drilling fluids play

several roles in drilling operations, and practically, all drilling difficulties are caused by drilling fluid parameters, either directly or indirectly.[4,5] Drilling fluids are anticipated to carry drilling cuttings and minimize fluid loss, among so many other things.

Both of these characteristics of drilling mud performance are impacted by the rheology of the fluid.[6,7] There is a direct relationship between carrying capacity and rheological features in water-based mud. Water-based drilling fluids (WDFs) with a
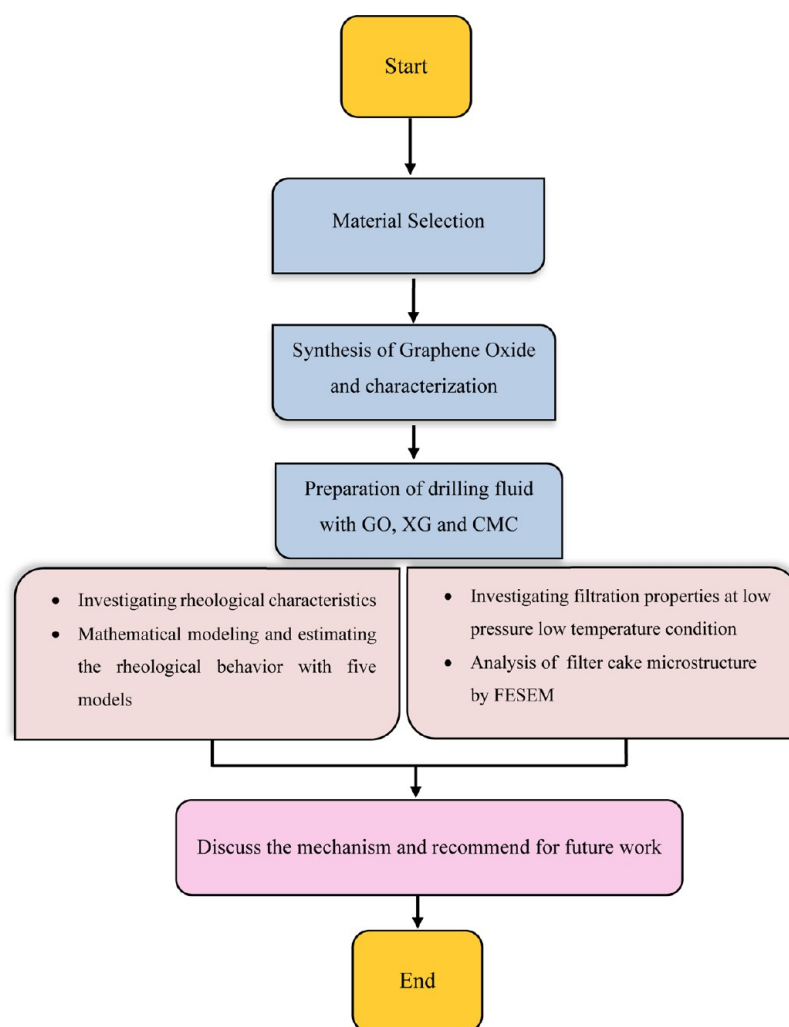
Figure 1. Experimental procedure flowchart of the current work.

greater viscosity and yield stress have a better conveying capability in general.[8] The filtration characteristics of WDFs have a significant impact on the wellbore's stability. Water infiltration into porous formations compromises wellbore stability and can result in significant challenges such as stuck piping and the collapse of formations.[9,10] As a basis, the rheological and filtration properties of WDFs are crucial factors in ensuring safe and successful drilling. In recent years, some natural[11−14] and synthetic[15−18] polymers were introduced as viscosifier and fluid loss controllers in water-based mud and were adopted worldwide in terms of cost and environmental impact.

Several nanotechnology applications in the petroleum industry have so many major benefits, particularly in drilling operations. Drilling problems can be decreased by utilizing ultrafine particles in drilling mud.[19−22] It has been proven that nanoparticles exhibit significant chemical and physical characteristics when they are put into the fluid as an additive due to their molecular properties.[23,24] However, few studies are conducted when nanoparticles, particularly, graphene oxide (GO), are used as the major component of drilling mud.

In addition to the size of nanoparticles, the study of their type, stability, and concentration is also critical. These materials are susceptible to any pH, temperature, and ionic strength.[25,26] Individual nanoparticles will attract each other,

generating aggregates that might significantly impair the drilling fluid's rheological and filtration characteristics due to poor colloidal stability or an excessive concentration.[27,28] Nanoparticles have been used in drilling fluids for various purposes, including viscosity stabilization, wellbore strengthening in shale, reducing water invasion into a borehole, loss circulation prevention, minimizing clay swelling,[29] and preventing the pipe from being stuck.[30−34] To achieve these purposes, many additives are utilized, such as carbon nanotubes,[35] GO,[21] zinc oxide,[36] nanosilica,[37−39] and CMC nanoparticles.[40,41] One of the widely explored nanoadditives that have a crucial impact on the performance of drilling fluids is graphene and its derivatives. Graphene is an atom-thick, 2D-conjugated structure with high conductivity and a huge surface area. Some reports showed that graphene-based materials presented fluid loss-controlling impact in WDFs.[21] Some of the patents also claim that graphene can be used to manage the swelling of shales. Because of its flexible sheet-like structure, graphene can plug the shale surface, preventing water from interacting with the shale and avoiding shale swelling.[42,43] It can also increase the life cycle of drilling a bit, lubricating the down-hole assemblies by penetrating the microscopic pores and creating a protective film on their surface.[44] Although several studies have been conducted on the size, type, and concentration of graphene-derivatives, additional research is
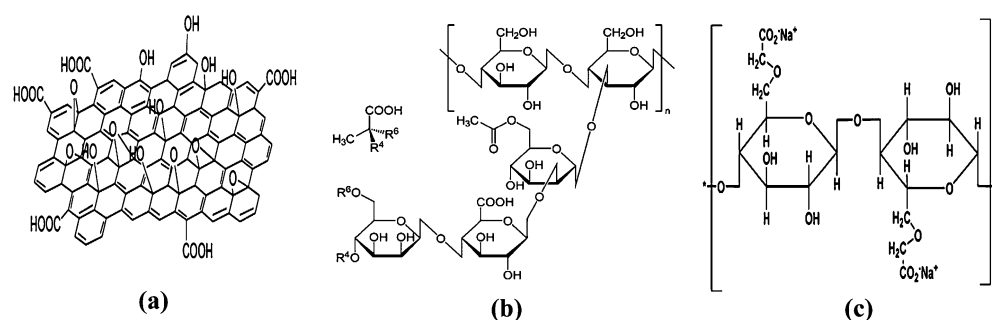
Figure 2. Structure of (a) GO,[48] (b) XG,[49] and (c) CMC.[50]

still required to understand various circumstances better. Drilling mud with fewer suspended particles has also increased penetration rates and reduced harmful environmental effects.[45,46]

Unlike previous studies, which utilized bentonite as the main component of drilling mud, in this research, we tried to prepare low-solid content mud using GO platelets to form a thin, strong, and impermeable filter cake by decreasing the fluid loss into formations. The new water-based mud was formulated by incorporating GO, xanthan gum (XG), and low-viscosity carboxymethyl cellulose at different concentrations. The rheological and filtration behavior of new mud in relation to additive concentrations was quantified, and the optimal concentration of GO was investigated. We applied five models to estimate the rheological behaviors of various fluids and investigated the filtration properties and filter cake microstructure of the GO/XG/CMC LV-WDF at low temperatures and low-pressure conditions.

On the other hand, the effects of other drilling additives could be investigated, and new mud could be evaluated under a broad range of temperature, pressure, and different PH conditions. There are also some mathematical models to estimate the shear stress and shear rate relationship, and comparing these models is a separate work. These issues are critical but beyond the scope of this work and will be intended for future work.

The current work is divided into various sections. First, the materials and methods utilized in the experiments are presented. The collected findings are then displayed. After that, the mechanism and modeling behind the rheological and filtration characteristics of fluids are shown. Finally, conclusions and recommendations are made based on the obtained results. The experimental procedure flowchart is presented in Figure 1.

2. MATERIAL AND METHODS

2.1. Materials. GO, XG, and low-viscosity carboxymethyl cellulose were employed to make WDFs. Graphene is a carbon with a honeycomb lattice on an atomic scale. GO (Figure 2a) is synthesized from graphite powder and has a sheet-like structure. The carbon plane is heavily adorned with hydroxyl groups, extending the interlayer distance and making these layers hydrophilic.[47]

2.1.1. Preparation of GO. Stable, water-dispersed GO was made using a modified Hummers approach.[51−55] First, natural graphite flakes (1 g) were quickly stirred in a mixture of $NaNO_3$ (0.5 g) and concentrated H_2SO_4 (80 mL, >98%, Merck) for 30 min. Afterward, 3 g of $KMnO_4$ (>99%) was gradually put into the mixture and agitated for 24 h at room temperature (20 °C). After that, the oxidation process was terminated by reacting the fluid mixture with a 400 mL aqueous solution of H_2O_2 (>30%). Then, to eliminate ions and other contaminants from the graphite oxide mixture, a series of centrifugation and washing processes with HCl aqueous solution (1 M) and deionized water was repeated multiple times. Finally, the layers were exfoliated for 30 min using sonication, followed by 10 min centrifugation at 9000 rpm to remove any unexfoliated particles. The sheet-like structure of GO platelets used in this study is shown in Figure 3.
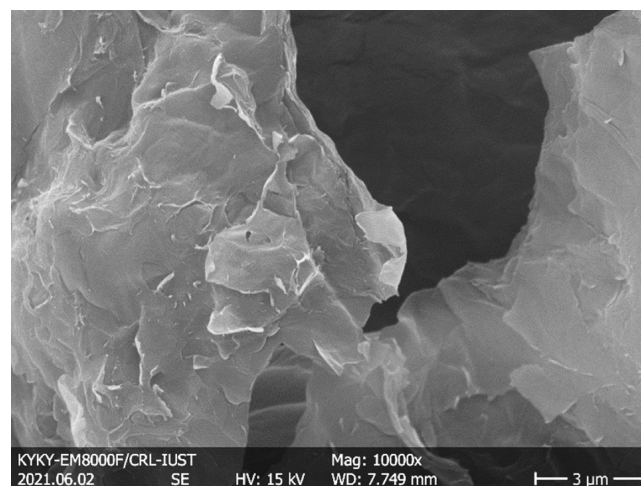

Figure 3. FE-SEM image of GO platelets.

2.1.2. Xanthan Gum. XG is a five-ring structure polymer and has thixotropic properties because of a particular branching structure. Figure 2b depicts a three-ring side chain with a two-ring backbone and functional groups such as carbonyl and hydroxyl. XG has a molecular weight of about 2 million g/mol, is soluble in water, and exhibits extremely pseudoplastic behavior. Hydrogen bonds can develop among polymer branches. When shear is applied, they will break because of the weak strength of bonding. The hydrogen bonds will form afterward under low shear rate situations, and viscosity will return to its initial state. XG is a typical viscosifier that improves dispersion stability in WDFs.[56,57]

2.1.3. Carboxymethyl Cellulose. CMC is made up of carboxymethyl groups (CH_2−COOH) linked to some of the hydroxyl groups. It is a polyelectrolyte with a linear structure (Figure 2c) derived from cellulose and made when cellulose reacts with the sodium salt of monochloroacetic acid ($ClCH_2$−COONa). CMC's three classes are used in drilling fluids (e.g.,

Table 1. Formulation of GO/XG/CMC LV WDFs

samples	set 1				set 2			set 3		
GO (wt %)	0	0.05	0.1	0.15	0.1	0.1	0.1	0.1	0.1	0.1
XG (wt %)	0.15	0.15	0.15	0.15	0	0.15	0.3	0.15	0.15	0.15
CMC LV (wt %)	0.15	0.15	0.15	0.15	0.15	0.15	0.15	0	0.15	0.3

CMC high, medium, and low viscosity) based on the degree of substitution.[58]

2.2. Drilling Fluid Formulation. Nine mud samples were produced using GO, XG, and CMC LV to study the impact of concentration on drilling fluid's rheology and filtration characteristics. These samples were categorized into three sets of fluids under the API standard procedure.[59] Four GO concentrations from 0.0 to 0.15 wt % were used in set I, while CMC LV and XG concentrations were fixed at 0.15 wt %. In set 2, three XG concentrations were employed, ranging from 0.0 to 0.3 wt %, whereas GO and CMC LV concentrations were fixed at 0.1 and 0.15 wt %, respectively. Finally, set 3 utilized three concentrations of CMC LV similar to the second data set, and the concentrations of GO and XG were assigned again at 0.1 and 0.15 wt %. The formulation summary at various concentrations is shown in Table 1.

2.3. Rheological Measurement. A six-speed rotating viscometer (Fann 35A Instrument Company) was utilized to characterize the rheological properties of the GO/XG/CMC LV-WDF. The viscometer was calibrated before being used for this work. At atmospheric conditions, the accuracy of this model is within ± 0.5 of dial reading. The following equations (eqs 1–3) were employed to calculate the rheological parameters of drilling mud.[45]

$$AV = \frac{\theta_{600}}{2} \tag{1}$$

$$PV = \theta_{600} - \theta_{300} \tag{2}$$

$$YP = \theta_{300} - PV \tag{3}$$

where AV denotes apparent viscosity, PV stands for plastic viscosity, and YP is the yield point. The dial readings at 600 and 300 rpm are also displayed in the form of θ_{600} and θ_{300}, respectively.

2.4. Rheological Modeling. Rheological modeling aims to estimate the relationship between shear stress and a shear rate of fluids with mathematical correlations. In this study, rheological data of the GO/XG/CMC LV-WDF fits the five models,[45] including Bingham-plastic, power-law, Casson, Herschel–Bulkey, and Sisko models. The Bingham-plastic model shows that the shear stress and shear rate have a linear relationship. The line intercept is yield stress, and the slope of the line is plastic viscosity. The model presents the relation between shear stress and shear rate in the following form (eq 4)

$$\tau = \tau_0 + \mu_p \dot{\gamma} \tag{4}$$

where τ is the shear stress, τ_0 denotes the yield stress, μ_p is the plastic viscosity, and $\dot{\gamma}$ shows the shear rate.

The power-law correlation is another two-parameter relation that describes the shear stress and shear rate relationship. This model is given in the following form (eq 5).

$$\tau = K\dot{\gamma}^n \tag{5}$$

where n is the flow behavior index and K denotes the flow consistency coefficient.

Some research is carried out to combine the $\tau/\dot{\gamma}$ non-linear relationship and yield stress concept. These studies result in more complicated models such as the Casson model (eq 6).

$$\sqrt{\tau} = \tau_0 + K\sqrt{\dot{\gamma}} \tag{6}$$

Three or more parameter models were proposed for more complicated fluids. By merging the enhancements of Bingham plastic and power law, valuable three-parameter correlations were developed. One of the most common models is Herschel–Bulkey, and it can describe the rheological characteristics of numerous drilling mud.[60] This model has the following form (eq 7)

$$\tau = \tau_0 + K\dot{\gamma}^n \tag{7}$$

Several studies were performed on lubricating greases to characterize their rheological behavior. Subsequently, these efforts led to developing the Sisko model for more complex fluids.[61] This model incorporates the concept of viscosity at an infinite shear rate and is given in the following form (eq 8)

$$\tau = \mu_\infty \gamma + K\dot{\gamma}^n \tag{8}$$

where μ_∞ denotes the infinite shear rate.

2.5. Filtration Measurement. Filtration experiments were conducted in accordance with API recommendations.[59] All tests were carried out under atmospheric conditions using Whatman quantitative ashless filter paper, grade 42 (particle retention size = 2.5 μm). A standard API filter press (Series 300 filter press, Fann Instrument Company), filter papers, a graduated cylinder, and a timer were used in the test. In addition, the instruments were meticulously calibrated prior to the measurement. The volume of the filtrates was recorded every 2.5 min from 1.0 to 30.0 min. Solutions were put in the filter cell under a pressure of 100 psi (690 kPa) with compressed air across a filter paper. After that, we removed the filter paper, gently rinsed it, and laid it out for 24 h under atmospheric conditions to allow the water molecules in the mud cake to evaporate. To keep the filter paper from curling while drying, a weight was put onto its edges.

The main tests of current work are rheological and filtration measurements and were performed under room conditions. We followed the American petroleum institute procedure to improve the accuracy and control the uncertainty to an acceptable limit of 2%. There are some influential factors in the uncertainty of the experiments such as the impurity of the material and cleanness of the laboratory supplies, the accuracy of the digital balance (± 0.01 gr), the accuracy of the viscometer (± 0.5 of dial reading), the pressure applied to the filter cell (± 5 psi), and reading the filtrate volume in nearest ± 0.1 mL.

2.6. FE-SEM Analysis. The obtained filter cake was left to dry for 5 days under atmospheric conditions. Then, the surface microstructure of the dried filter cake was studied using FE-SEM (KYKY-EM8000F/CRL system, China) with a 15 kV
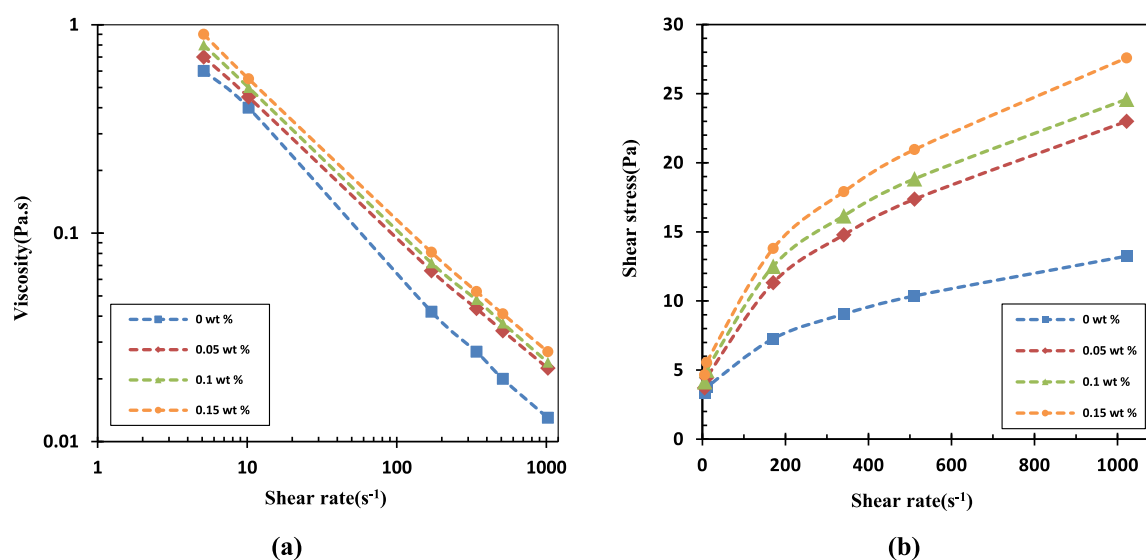
Figure 4. Plots of (a) viscosity and (b) shear stress versus shear rate for GO/XG/CMC LV-WDF at various GO concentrations.

accelerating voltage. Before the analyses, the items were spin-coated with gold.

3. RESULTS AND DISCUSSION

3.1. Fluid Rheological Properties. Rheology and filtration properties of drilling fluids depend on parameters such as the concentration of additives and the temperature of the drilling fluids.[62] Increasing the polymer concentration can decrease the API fluid loss noticeably. Polymers also contribute to the formation of the network structure, which results in the capacity to build up viscosity. The rheological property of drilling mud then altered as the polymer concentration increased.

An increase in temperature causes the main chain of the polymeric molecule to be broken. Then, the value of API fluid loss of the drilling fluid increased. On the other hand, the rheological property of the drilling fluid decreases as the temperature increases.[63] Some polymers degraded at high temperatures, breaking up the network structure to a certain extent. Nevertheless, this negative influence is held within limits and controlled by some other additives.[64] In this research, we investigate all the experiments under atmospheric conditions. Therefore, the temperature variation was not considered. However, the effect of concentration should definitely be recognized.

The plot of viscosity as a function of shear rate for GO/XG/CMC LV-WDF is shown in Figure 4a. The concentration of GO in the solution was changed from 0.0 to 0.15 wt % to evaluate the impact of GO on the rheological properties, and the concentrations of XG and CMC LV were constant (0.15 wt %) for all fluids.

As shown in Figure 4a, adding a tiny amount of GO enhances the rheological property and the shear-thinning behavior improves. Drilling mud with good shear-thinning properties is easier to be pumped into the bottom of the wellbore and is widely yearned in a drilling operation. With this outstanding feature of GO, it could be a better component for tuning fluid flow behaviors. Without GO, the XG/CMC LV suspension even displayed a nearly shear-thinning property, proving that the XG additive may be employed as a strong viscosifier in drilling mud.[65] GO concentrations and shear rates

influenced the shear stress (Figure 4b). When the GO concentration increases from 0 to 0.15 wt %, the shear stress steadily rises. For instance, the shear stresses of GO/XG/CMC LV-WDF with 0.0, 0.05, 0.1, and 0.15 wt % of GO are 13.24, 22.98, 24.61, and 27.58 Pa, respectively, at a high shear rate of 1022 s^{-1}. Shear stress in the presence of 0.15 wt % GO is double that in the absence of GO at a high shear rate. Rheological analysis confirmed that the GO concentration influenced the rheological characteristics of GO/CMC LV/XG in a good way. The sheet-like shape of GO is well known. Carboxyl and hydroxyl groups were found on the edges and planes of the GO sheets, respectively.[66] GO plates were well distributed in a water suspension. Because of the existence of functional groups, XG and CMC LV are also negatively charged. Consequently, a hydrogen bond between XG/CMC LV and GO can be developed due to many hydroxyl groups on XG and CMC LV chains. As more XG and CMC LV were added to the GO solution, the bonding structure became substantially stronger, resulting in a higher flow resistance upon shear rate, indicating the continually rising viscosity and shear stress.

Mud density, plastic viscosity, and yield point are essential parameters for determining the rheological behaviors of drilling fluids that help to maintain formation pressure and enhance wellbore stability. Low mud density can cause rock shear failure, also known as wellbore breakout, which can cause the wellbore to collapse. However, high mud density may result in the loss of circulation, a decrease in penetration rate, and formation damage. The weight of mud is almost unaffected by adding nanoadditives to WDFs.[67] As a result, the mud weight impact was not taken into account in this study.

Plastic viscosity is the flow resistivity produced by friction between solid particles in drilling fluids and fluid layers. It is determined by the viscosity of the base fluids and the solid content. In essence, higher PV arises from increased mud weight or solid content in drilling fluids, which is undesirable since it reduces drilling speed. The adverse effects of PV have been mitigated by adding water or a thinner to drilling mud.[68] The addition of 0.05 wt % of GO could increase the plastic viscosity of GO/XG/CMC LV-WDF from 6 to 11 centipoise. The dimension, shape, number of particles, and liquid-phase
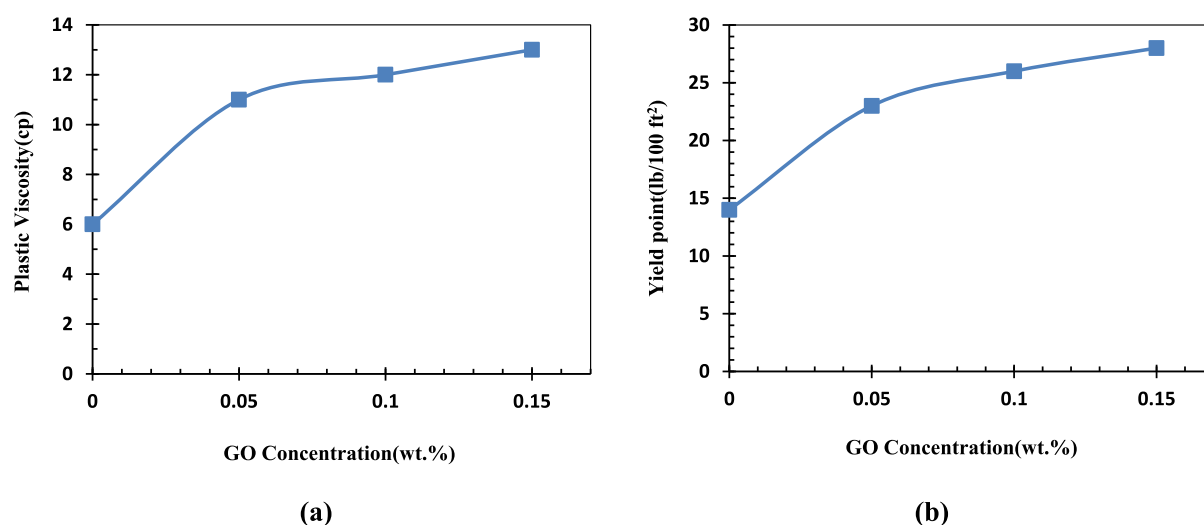
(a)   (b)

Figure 5. Plot of (a) plastic viscosity and (b) yield point versus different GO concentrations.

Table 2. Rheological Parameters for GO/XG/CMC LV at Various GO Concentrations Using Different Models

models		GO concentrations (wt %)			
		0	0.05	0.1	0.15
Bingham-plastic	τ_0	8.9464	11.8739	13.3416	14.7056
	μ_P	0.0186	0.0363	0.0383	0.04311
	R^2	0.9129	0.9050	0.8937	0.8906
	SSR	7.2339	26.8706	33.9417	38.9495
	RMSE	1.3448	2.5918	2.9129	3.1204
power law	K	1.7525	1.8337	2.0787	2.2532
	n	0.3800	0.3690	0.3545	0.3489
	R^2	0.9661	0.9775	0.9879	0.9875
	SSR	1.0796	0.7748	0.7711	0.7663
	RMSE	0.5195	0.4401	0.4316	0.4182
Herschel−Bulkley	τ_0	2.2941	1.6545	1.6188	2.1225
	K	0.5186	0.9959	1.2828	1.2466
	n	0.4400	0.4323	0.4163	0.4053
	R^2	0.9974	0.9998	0.9996	0.9999
	SSR	0.2678	0.0487	0.0261	0.0088
	RMSE	0.2187	0.1804	0.1770	0.0470
Casson	τ_0	1.8415	2.0316	2.1693	2.2720
	K	0.0585	0.0901	0.0913	0.0973
	R^2	0.9793	0.9762	0.9713	0.9757
	SSR	1.5503	6.8613	9.3163	9.8698
	RMSE	0.6225	1.3097	1.5261	1.5708
Sisko	μ_∞	0.0033	0.0041	0.0033	0.0049
	K	2.0213	2.1531	2.4113	2.7506
	n	0.3592	0.3326	0.3133	0.3037
	R^2	0.9971	0.9997	0.9992	0.9998
	SSR	0.2127	0.0725	0.2249	0.0446
	RMSE	0.2306	0.2146	0.1771	0.1056

viscosity influence plastic viscosity.[69] Graphene plates distribute throughout the fluid due to their vast surface area, necessitating additional liquid phases to wet their surfaces. As a result, the plastic viscosity and carrying capacity will increase efficiently (Figure 5a).

The degree of non-Newtonian drilling fluids is measured with the yield point parameter. It is the capacity to keep drill cuttings suspended in the wellbore while cycling in and out of the annulus. As a result, drilling issues such as differential sticking can be avoided. The YP rises as the size of the solid additive particles decreases. This is due to enhanced attraction forces between solid particles, which increases drill cutting carrying capacity and cleans the wellbore.[70]

It can be observed in Figure 5b that GO/XG/CMC LV-WDF with 0, 0.05, 0.1, and 0.15 wt % of GO has yield points of 14, 23, 26, and 28 lb/100 ft², respectively. Drilling engineers utilize the yield point concept (force necessary to initiate the flow) to anticipate the capability of drilling mud to convey cutting during operation. As previously stated, adding GO to a solution can improve its electrochemical behavior and positively impact long-chain polymers like XG. As a result of the rheological findings, the introduction of GO also increased
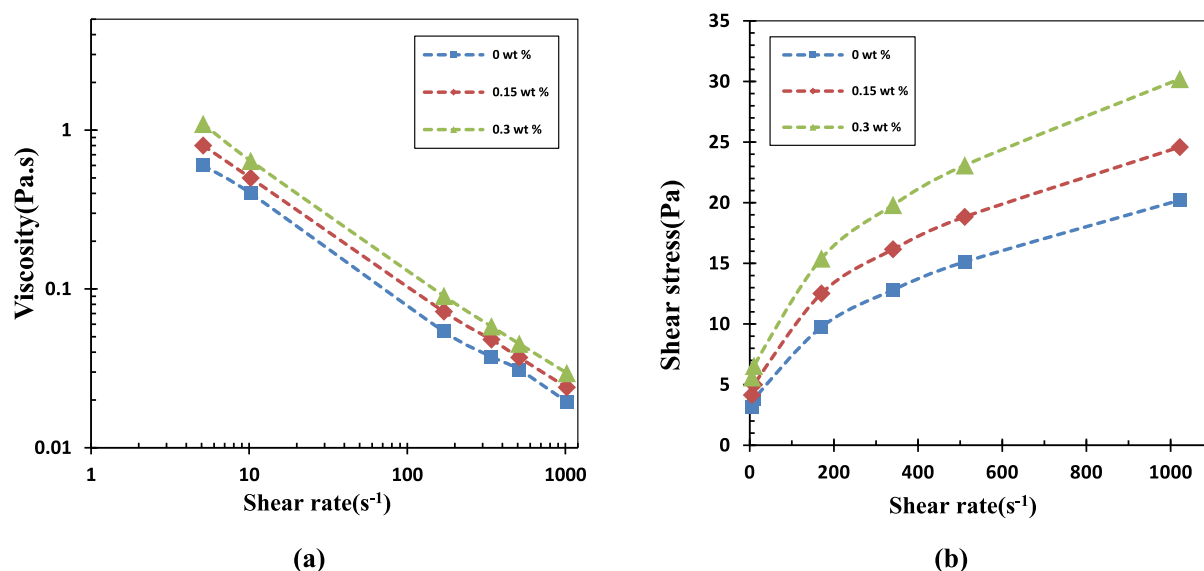
Figure 6. Plots of (a) viscosity and (b) shear stress vs shear rate for GO/XG/CMC LV-WDF at various XG concentrations.

wellbore cleaning and cutting transport efficiency. The recommended plastic viscosity and yield points proposed are 15−40 cP and 5−12.5 lb/100 sq. ft,[71] respectively; Therefore, our GO solutions possess adequate rheological properties. Additive concentrations in all formulations are less than 2 wt %, categorized as low-solid drilling mud.[72] High drilling speed, thin filter cake, and reduced friction on pumping facilities are the advantages of employing low-solid drilling fluids.[8]

Experimental results were matched with different models, such as Bingham-plastic, power-law, Casson, Herschel−Bulkey, and Sisko models, to determine the relationship between shear stress and shear rate. The list of matching parameters is shown in Table 2. According to the values of fitting parameters such as R^2 (greater than 0.99), SSR (less than 1), and RMSE (less than 0.2), the satisfactory model is determined for characterizing the rheological properties of water-based mud at various GO concentrations. Because the Bingham-plastic model exhibits a linear relationship, it was ineffective in describing the rheological behavior of non-Newtonian fluids like GO/XG/CMC LV-WDF. As shown in Table 2, the R^2 continuously declined from 0.9129 to 0.8906 when the GO concentration rose from 0 to 0.15 wt %. At the same time, the SSR/RMSE values increased from 7.2339/1.3448 to 38.9495/3.1204, respectively, showing the nonlinear relationship between rheological parameters. The power law fits better than the Bingham-plastic correlation, illustrating the nonlinear correlation once more. The R^2 values vary smoothly from 0.9661 to 0.9875, and the SSR/RMSE values changed from 1.0796/0.5195 to 0.7663/0.4182, respectively. The resulting R^2 parameter, nevertheless, is less than 0.99, necessitating complicated three-parameter correlations to characterize the rheological behavior accurately.

The Casson model appears to be well suited at low GO concentrations relative to high concentrations. However, the Casson model still worked weakly with an R^2 value of 0.97 (less than 0.99), SSR values of 1.5503 to 9.8698, and RMSE values of 0.6225 to 1.5708. In this study, Herschel−Bulkey and Sisko models were utilized as three-parameter rheological models. They precisely fitted the rheological curves of GO/XG/CMC LV-WDF at nearly all GO concentrations. The Herschel−Bulkey correlation with the greatest R^2 (0.9999),

smallest SSR (0.0088), and RMSE (0.0470) best approximated the rheological characteristics of GO/XG/CMC LV-WDF. There are also some other mathematical models to estimate the shear stress and shear rate relationship, and comparing these models needs additional research.

The Herschel−Bulkey model (integration of Bingham-plastic and power-law) represents the most accurate fit for the rheological behavior of GO/XG/CMC LV-WDF in this investigation. The parameters such as yield point (τ_0), flow behavior index (n), and consistency coefficient (K) provide more valuable information. The rheological parameters such as τ_0, n, and K were all affected by the concentration of GO (Table 2). The values of n were less than one, indicating that the drilling fluids were shear-thinning. The increase in GO concentration leads to improved cutting transportation as the τ_0 gradually increases. However, because the τ_0 also denotes the minimum stress required to commence flow, if the τ_0 is exceptionally high, it will take a lot of energy to transfer the drilling mud into the borehole.[73] Increasing the GO concentration consistently increased the amounts of K, implying that at higher GO concentrations, the shear stress dependency on the shear rate is more than those at smaller amounts of GO. The n value, on the other hand, continually dropped as the GO concentration increased, showing that higher GO concentrations resulted in more dramatic shear-thinning fluids.

Figure 6a indicates the viscosity versus shear rate graph for GO/XG/CMC LV-WDF at different XG concentrations. To describe the impact of XG on the rheological behavior, the XG concentration was selected to 0.0, 0.15, and 0.3 wt % and the constant CMC LV and GO concentration for all fluids was set to 0.15 and 0.1 wt %, respectively.

Zero concentration XG produced a similar shear-thinning curve. The addition of XG improved the rheological and shear-thinning manner of drilling mud. Figure 6a revealed the importance of XG in increasing the viscosity of GO/CMC LV/XG. In the absence of XG, the bonding between functional groups of GO, CMC LV, and water molecules is relatively weak. Accordingly, the curve shows a similar shear-thinning behavior. By adding more XG, a long-chain polymer structure was formed, and surface interaction was improved; thus, the

linear shear thinning behavior of the GO/XG/CMC LV-WDF with 0.15 and 0.3 wt % of XGs was demonstrated.

Besides, the GO/XG/CMC LV-WDF's viscosity also increased with XG incorporation from 0.0 to 0.3 wt %.

Addition of XG from 0.0 to 0.3 wt % resulted in the gradual increase of the shear stress of GO/XG/CMC LV-WDF (Figure 6b). For example, the shear stress of GO/XG/CMC LV-WDF increased from 20.21 Pa at 0.0 wt % of XGs to 24.59 and 30.21 Pa at 0.15 and 0.3 wt % of XGs, respectively, at a high shear rate of 1022 s^{-1}.

Table 3 contains the matching parameters. Bingham-plastic and Casson correlations were inappropriate to describe the

Table 3. Rheological Parameters for GO/XG/CMC LV at Various XG Concentrations Using Different Models

models		XG concentrations (wt %)		
		0	0.15	0.3
Bingham-plastic	τ_0	10.1849	13.3416	16.9459
	μ_p	0.0320	0.0383	0.04629
	R^2	0.9036	0.8937	0.9012
	SSR	21.1950	33.9417	45.6160
	RMSE	2.3019	2.9129	3.3769
power law	K	1.4519	2.0787	2.7605
	n	0.3773	0.3545	0.3422
	R^2	0.9925	0.9979	0.9843
	SSR	0.7171	1.7311	2.7833
	RMSE	0.1590	0.4216	0.8341
Herschel−Bulkley	τ_0	1.5646	1.6188	2.8764
	K	0.7707	1.2828	1.3366
	n	0.4597	0.4463	0.4355
	R^2	0.9954	0.9996	0.9999
	SSR	0.1927	0.1261	0.0978
	RMSE	0.2981	0.1875	0.1742
Casson	τ_0	1.8755	2.1693	2.4586
	K	0.0851	0.0913	0.0991
	R^2	0.9730	0.9713	0.9752
	SSR	6.0315	9.3163	11.6114
	RMSE	1.2279	1.5261	1.7037
Sisko	μ_∞	0.0035	0.0033	0.0061
	K	1.7886	2.4113	3.4340
	n	0.3207	0.3133	0.2809
	R^2	0.9942	0.9972	0.9980
	SSR	1.2655	0.9249	0.2254
	RMSE	0.5624	0.4771	0.4357

rheological characteristics. At low XGs (until 0.15 wt %), the power-law model gave relatively sound prediction in the rheological data. However, when the amounts of XGs expanded to 0.3 wt %, the power-law model failed to characterize fluid rheological behaviors with an R^2 value of 0.98 (less than 0.99), SSR value of 2.7833, and RMSE value of 0.8341. Herschel−Bulkey and Sisko models were fitted and described the rheological behavior of GO/XG/CMC LV-WDF better than other models.

Nevertheless, the Herschel−Bulkey model was the best one with the most excellent R^2 in addition to the smallest SSR and RMSE. However, the concentration of XGs had a substantial effect on τ_0, n, and K. As shown in Table 3, when the XG concentration increased, τ_0 and K continuously expanded. In contrast, the amounts of n steadily declined. Such findings are consistent with the early discussed subject about the impact of GO concentrations.

Figure 7a shows the viscosity versus shear rate graph for GO/XG/CMC LV-WDF at various CMC LV concentrations with a constant proportion of XG and GOs to 0.15 and 0.1 wt %, respectively. The GO/XG/CMC LV-WDF had almost linear shear-thinning rheological curves at all CMC LV concentrations used.

The viscosity of GO/XG/CMC LV-WDF increased slightly as the CMC LV concentration expanded from 0.0 to 0.3 wt %. As shown in Figure 7a, three viscosity curves are close to each other and do not differ significantly. Thus, the CMC LV concentration has a minor impact on the viscosity of GO/XG/CMC LV-WDF than XGs. Compared to Figure 6a, the XG concentration has a more significant effect on the viscosity, which can be seen from the difference in the curves.

On the other hand, XG had a more significant impact on improving the rheological characteristics than CMC LV at the same concentrations. This might be attributed to differences in substitution degree, crystallinity functional group, dimension, and gel-forming ability. XG exhibited a strong hydrophilic behavior with a particular branching structure rather than the linear structure of CMC LV. Hydrogens can form strong bonds between polymer branches in XGs due to multiple carbonyl and hydroxyl functional groups. Therefore, when XG and CMC LV were introduced to an aqueous GO solution, it was predicted that XG would create more hydrogen bonds between its functional groups and water molecules than CMC LV. Additionally, XG displayed a high gel-forming ability due to its greater molecular weight and many hydroxyls on the chains. Hence, water molecules are enabled to link along these chains. When XG was added to the solution, it acted as a cross-linker, making the matrix's network structure robust and more interconnected. As a result, a tight network was formed between the GO layers, XG, and water molecules, which demonstrated high opposition to flow, resulting in a considerable enhancement in the rheological characteristics of fluid rather than CMC LV.

CMC LV increased the shear stresses of the GO/XG/CMC LV-WDF as well (Figure 7b). For example, the shear stresses of GO/XG/CMC LV-WDF with 0.0, 0.15, and 0.3 wt % of CMC LV were 22.53, 24.59, and 26.61 Pa, respectively, at a high shear rate of 1022 s^{-1}.

Table 4 summarizes the model parameters acquired. The Bingham-plastic, Casson, and power-law correlations are not appropriate to predict the behavior of GO/CMC LV/XG at any concentration of CMC LV. These findings indicate that GO and XG were primarily responsible for the complicated rheological behavior of GO/CMC LV/XG. The Herschel−Bulkey model fits the rheological behavior of GO/XG/CMC LV-WDF the best of the five rheological models at all CMC LV concentrations. In terms of rheological characteristics, Table 4 demonstrates that increased CMC LV concentrations, which resulted in greater τ_0 and K. The n value, on the other hand, is less affected by the CMC LV concentration. For instance, the amount of n acquired from the Herschel−Bulkey correlation is about 0.4. Drilling fluids with a high consistency index (K) value implies superior hole cleaning efficiency; therefore, a higher K value is appropriate for drilling operations. A reduction in the value n also indicates that the modified drilling fluid has a more excellent shear-thinning characteristic, which is favorable for optimal hole cleaning.[43] The rheology of GO/XG/CMC LV-WDF closely followed the shear-thinning behavior, regardless of the CMC LV content, and the level of shear-thinning attitude was less impacted by
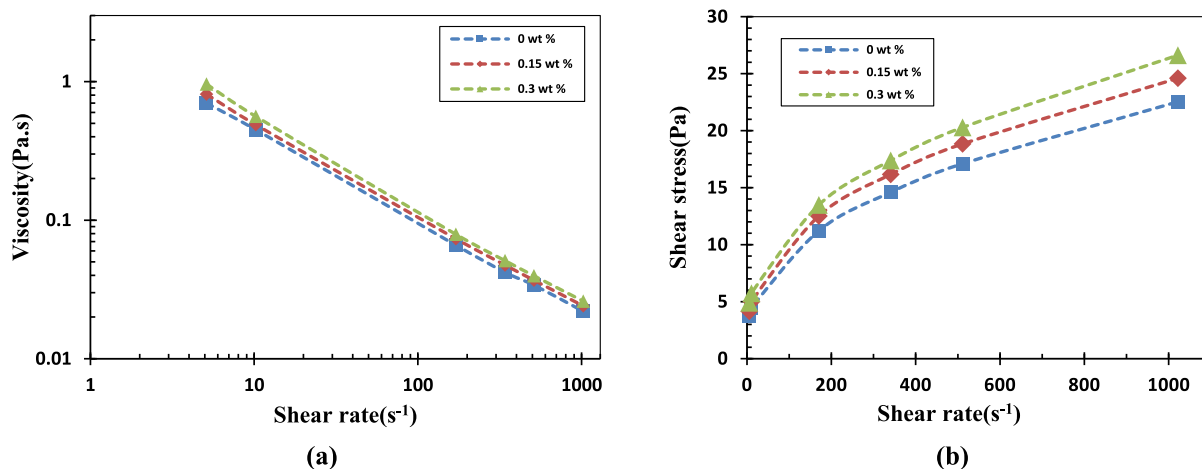
Figure 7. Plots of (a) viscosity and (b) shear stress vs shear rate for GO/XG/CMC LV-WDF at various CMC LV concentrations.

Table 4. Rheological Parameters for GO/XG/CMC LV at Various CMC LV Concentrations Using Different Models

models		CMC LV concentrations (wt %)		
		0	0.15	0.3
Bingham-plastic	τ_0	11.8525	13.3416	14.8153
	μ_p	0.03539	0.0383	0.0408
	R^2	0.9013	0.8937	0.9040
	SSR	26.6480	33.9417	34.4078
	RMSE	2.5810	2.9129	2.9329
power law	K	1.7877	2.0787	2.3906
	N	0.3633	0.3545	0.3445
	R^2	0.9971	0.9979	0.9952
	SSR	0.8507	0.7111	1.8849
	RMSE	0.4611	0.4216	0.6864
Herschel−Bulkley	τ_0	1.6084	1.6188	2.5904
	K	1.0320	1.2828	1.1266
	N	0.4343	0.4363	0.4385
	R^2	0.9992	0.9996	0.9991
	SSR	0.2043	0.2261	0.3172
	RMSE	0.2260	0.1775	0.1816
Casson	τ_0	2.0354	2.1693	2.2964
	K	0.0885	0.0913	0.0933
	R^2	0.9744	0.9713	0.9771
	SSR	7.0379	9.3163	8.3358
	RMSE	1.3264	1.5261	1.4435
Sisko	μ_∞	0.0038	0.0033	0.0055
	K	2.1607	2.4112	2.9984
	N	0.3111	0.3134	0.3011
	R^2	0.9991	0.9992	0.9989
	SSR	0.2364	0.2249	0.3688
	RMSE	0.2431	0.2371	0.3036

CMC LV concentrations. Furthermore, CMC LV had a minor influence on the rheological parameters as compared to GO and XGs, suggesting the more practical function of GO/XGs in increasing the rheological characteristics of GO/CMC LV/XG.

Herschel−Bulkley and Sisko models (three-parameter models) provided superior matching outcomes than two-parameter correlations for all GO/XG/CMC LV WDF formulations. At high solid content fluids, these occurrences become more prominent. However, there were certain drawbacks in the two-parameter models. In most cases, these restrictions resulted in inaccurate fitting data. The Bingham-plastic model, for example, consistently produced the highest τ_0 and the lowest R^2 values, suggesting unacceptable estimations, as seen in Tables 2−4 Therefore, it is encouraging to observe that the Herschel−Bulkley model produced the best prediction for GO/CMC LV/XG, independent of component concentrations. These findings are notable because they allow petroleum engineers to anticipate the viscosity and shear stress for GO/XG/CMC LV-WDF in all formulations at a given shear rate, improving the safety, efficiency, and cost of drilling operations. Although, for utilizing this formulation in deep reservoirs, the effects of high-pressure and high-temperature conditions should be evaluated in separate work.

3.2. Fluid Filtration Properties. Fluid penetration into the formation is commonly recognized to cause swelling and, as a result, wellbore collapse problems. Furthermore, the thick filter cake established on the borehole wall increases the pipe stuck risks and wellbore damages.[74] Accordingly, an efficient drilling fluid should have a little filtration volume and a thin, compact mud cake. API fluid loss experiments were employed to evaluate the filtration property of GO/XG/CMC LV-WDF at various GO, CMC LV, and XG concentrations. The obtained filtrate was colorless and had a relatively low viscosity for all samples, showing that water was the major component in the filtrate.

Moreover, the filtration rate was relatively high in the initial steps. The filtering rate significantly decreased as time passed. Figure 8a depicts the impact of GO concentration on the filtering characteristics of GO/CMC LV/XG. It is worth mentioning that without GO, no cake was made on the filter paper. As a result, after 1 min, all the water quickly flowed through the paper; therefore, zero concentration GO is not depicted in Figure 8a.

When GO was introduced, the volume of fluid loss was dramatically decreased because of creating and developing a narrow and compressed mud cake. GO plates clogged the paper pores, thereby restricting the permeation conduits. For instance, the API fluid loss of the GO/XG/CMC LV-WDF with 0.05, 0.1, and 0.15 wt % of GO was 15.4, 12.4, and 8.7 mL/30 min, respectively. As a result, GO was critical in avoiding fluid loss due to the generation of a superior barrier on the filter paper.

The impact of XG concentration on the filtering characteristics of GO/XG/CMC LV-WDF is shown in Figure 8b. Even in the absence of XG, the GO/CMC LV exhibited a fluid loss
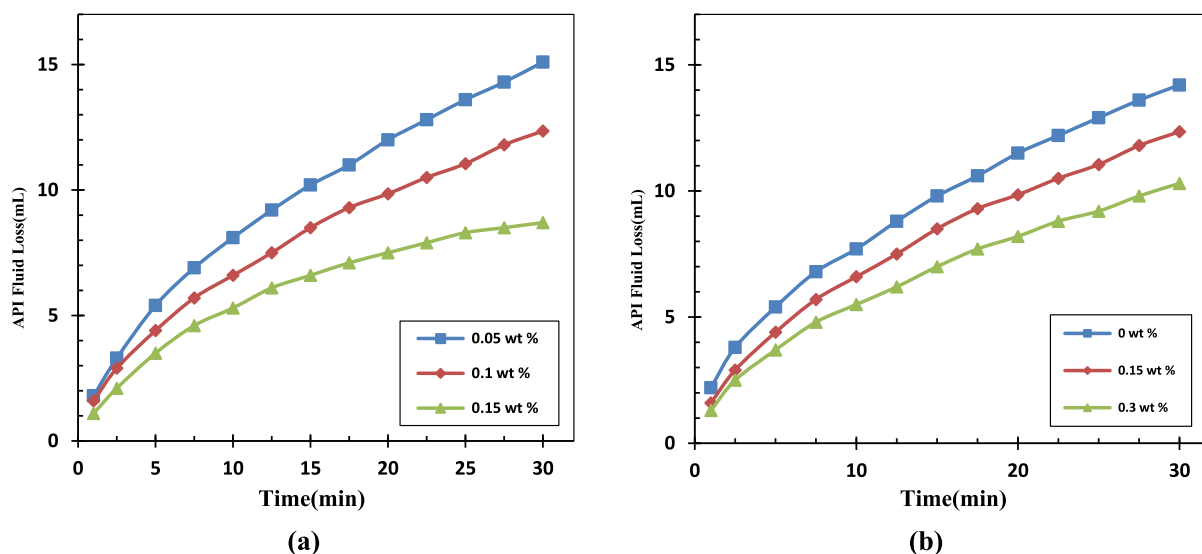
Figure 8. API fluid loss volume vs time for GO/XG/CMC LV-WDF at various (a) GO and (b) XG concentrations.
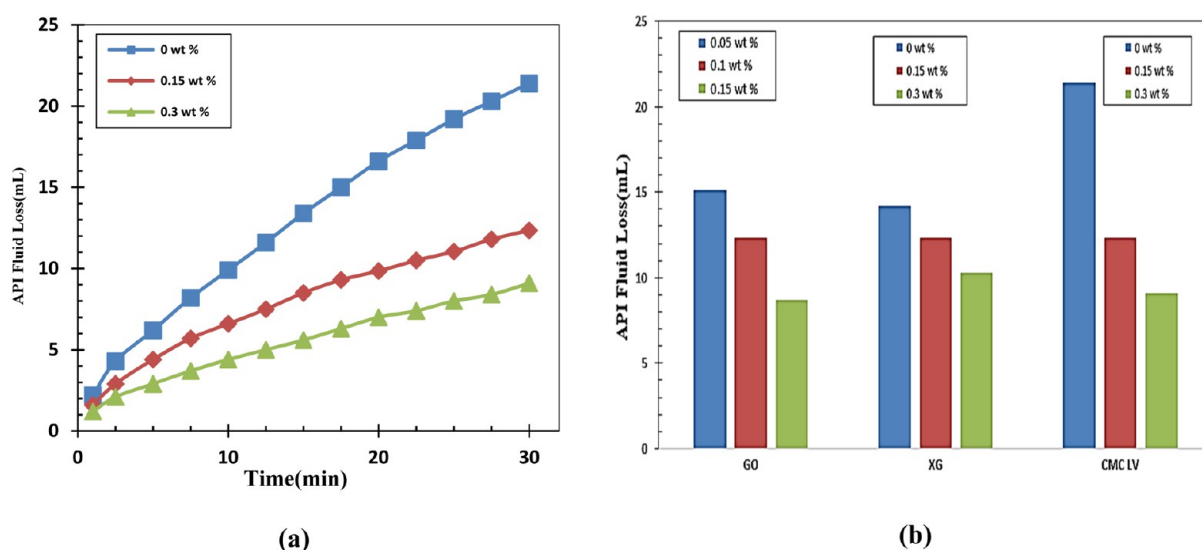

Figure 9. Plots of (a) API fluid loss volume versus time for GO/XG/CMC LV-WDF at various CMC LV concentrations. (b) API fluid loss volume for different GO, XG, and CMC LV concentrations at a time, 30 min.

of 14.2 mL at 30 min, demonstrating fairly good filtration, which would be lower than the suggested fluid loss value (15.0 mL) for water-based mud.[75] The addition of XG had no governing effect on fluid loss, but as a viscosifier, it can improve the filtration property by enhancing the gelling structure of the fluid. Figure 8b shows that the GO/XG/CMC LV-WDF with 0.0, 0.15, and 0.3 wt % XG had a fluid loss of 14.2, 12.4, and 10.3 mL/30 min, respectively.

Figure 9a depicts the influence of CMC LV concentration on GO/CMC LV/XG-WDF fluid loss. The API fluid loss volume of GO/XG-WDF without the addition of CMC LV was 21.4 mL/30 min, approximately one and a half greater than GO/CMC LV (14.2 mL/30 min), showing that CMC LV played a more vital role in enhancing the filtering property. On the other hand, the contribution of CMC LV to the filtration characteristics was prevailing than the XG portion (Figure 9b). The API fluid loss for the GO/XG/CMC LV-WDF with 0.0, 0.15, and 0.3 wt % of CMC LV was 21.4, 12.4, and 9.1 mL/30

min, respectively, indicating a downward trend with increasing CMC LV concentration.

Figures 10 and 11 display the photographs of fresh and dried filter papers after 24 h at room temperature. In the observation, we can see that the filter cake color moderately varied from light brown to dark black because of more significant amounts of GO being precipitated on the paper by addition of GO at concentrations from 0.05 to 0.15 wt % (Figure 10) and the filter cake became dense, thin, and compact.

Without GO, no cake was formed on the filter paper and all XG/CMC LV solutions flowed through the filter paper (Figure 11a,å). This indicates that GO plates have plugging effects and can block the permeation channels on the filter paper.

The filter cake of GO/XGs has a lighter color than GO/CMC LV, and its structure becomes looser toward the margin of the filter paper (Figure 11b,c,b̊,c̊). This shows that the CMC LV molecules can bind to the graphene plates better than XG molecules.
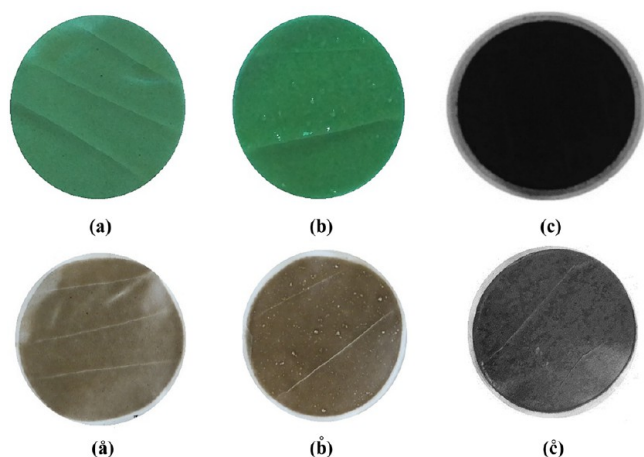
Figure 10. Photographs of fresh filter cake: (a) 0.05 wt %, (b) 0.1 wt %, and (c) 0.15 wt % of GO at 0.15 wt % concentration of XG and CMC LV. Photographs of the same filter cake after drying 24 h under atmospheric conditions (å−c̊).

Figure 11d,d̊ indicates that without XG and CMC LV, GO solution, even at a concentration of 0.15 wt %, formed loose, thick, and open filter cakes that disintegrate after 24 h of drying at room temperature. Thus, XG and CMC LV had a significant role in bridging the graphene plates and making them a stiff barrier on filter paper.

Filtration experiments revealed that when GO and CMC LV concentrations increased, the API fluid loss of GO/XG/CMC LV-WDF reduced noticeably, whereas XG had less impact on the fluid loss. According to prior research,[74] the fluid viscosity and filter cake characteristics were the critical determinants of filtration property. Increased fluid viscosity slows the filtering rate in general.[76] However, rheological studies (Figures 4−7) revealed that the viscosity of GO/XG/CMC LV-WDF rose significantly as GO and XG concentrations increased but only somewhat when CMC LV concentrations increased. Thus, the rheological behavior at various XG and CMC LV concentrations contradicted the results of fluid loss testing. The findings indicate that the filtrate volume in GO/CMC LVs is smaller than that in GO/XG fluids but the viscosity of GO/CMC LV is unexpectedly lower than that of GO/XGs. Hence, the microstructure of the filter cake should be studied to

discover the cause of this discrepancy. The alteration in the morphology of filter cakes was seen using FE-SEM observations at different concentrations of GO, XG, and CMC LV.

The effect of GO concentrations on the surface morphologies of filter cakes at a constant concentration of XG and CMC LV (0.15 wt %) is shown in Figures 12−14. The
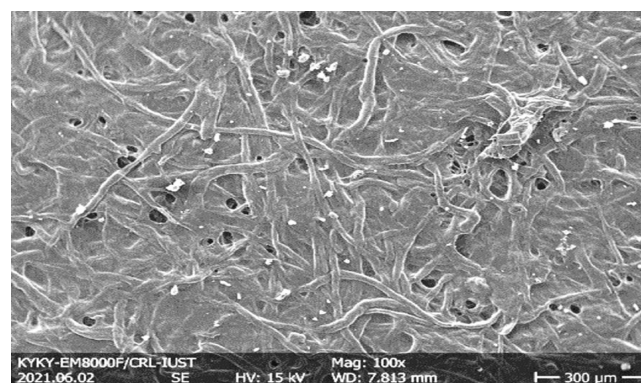

Figure 12. FE-SEM image of dried filter cake formed by the 0.05 wt % of GO deposited on filter paper (concentrations of XG and CMC LV are 0.15 wt %).
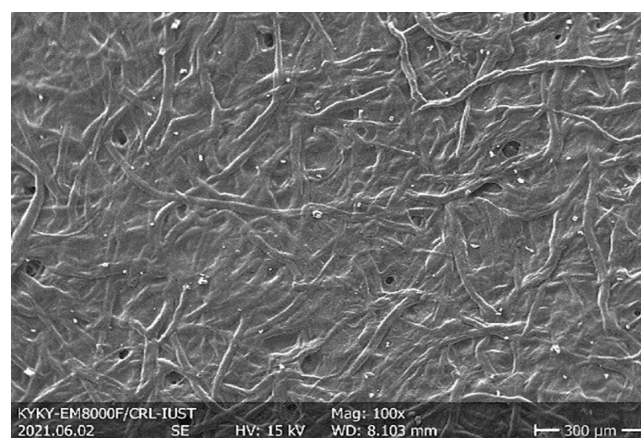

Figure 13. FE-SEM image of dried filter cake formed by 0.1 wt % of GO deposited on the filter paper (concentrations of XG and CMC LV are 0.15 wt %).
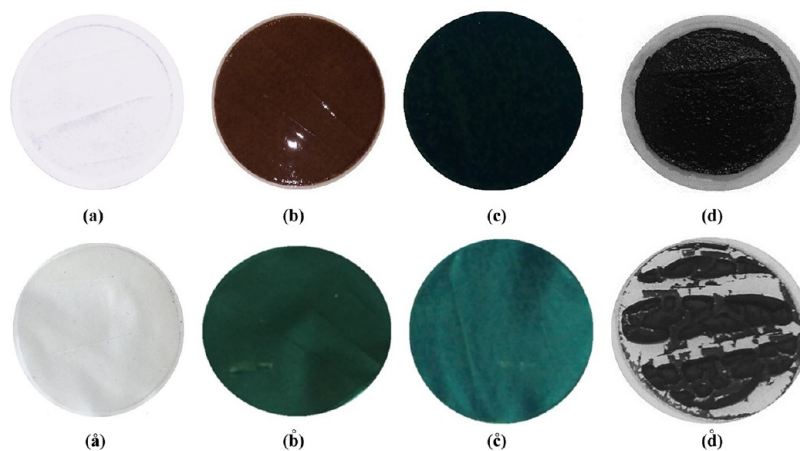

Figure 11. Photographs of fresh filter cake: (a) XG/CMC LV-0.15 wt %, (b) GO/XG-0.15 wt %, and (c) GO/CMC LV-0.15 wt %, and (d) GOs/0.15 wt %. Photographs of the same filter cake after drying 24 h at room temperature (å−d̊).
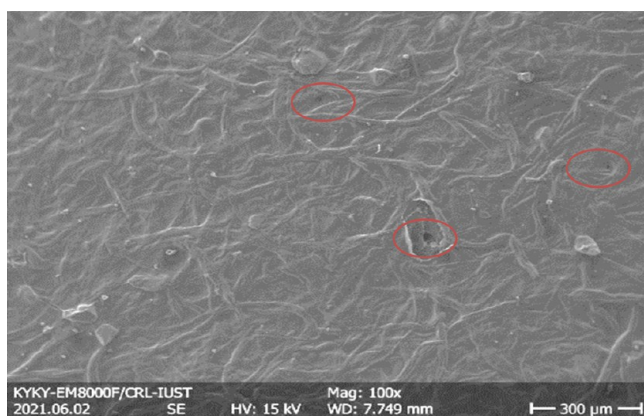
Figure 14. FE-SEM image of dried filter cake formed by 0.15 wt % of GO deposited on the filter paper (concentrations of XG and CMC LV are 0.15 wt %). The holes are shown with red circles.

Figure 15. FE-SEM image of the dried filter cake formed by 0.15 wt % of GO and XG.

API filter loss of the GO/XG/CMC LV-WDF was reduced by expanding the GO concentration from 0.05 to 0.15 wt %. The holes on the surface of the filter cake were easily observed when the concentration of GO was 0.05 wt % and the number of holes were reduced by increasing the GO concentration.

As discussed earlier, the viscosity of the fluid will increase as the GO concentration increases. The increased viscosity decreased the filtration rate, indicating that viscosity positively impacted filtration characteristics. The addition of XG (branched structure polymer) and CMC LV (linear structure polymer) to the GO solution may influence the microstructure of filter cake, resulting in a morphology similar to the plant roots in the ground. Because of the hydrogen bond among the oxygen-containing, carbonyl, and hydroxyl functional groups, GO platelets developed a dense filter cake on the paper at a different GO concentration. The strength of hydrogen bonding is related to the density of functional groups directly. Therefore, when these plates would not be dispersed in a layered manner somewhere, the discontinuity will have resulted in the barrier failure against water infiltration. Thus, some micropores were developed in the architecture of mud cake. When the concentration of GO plates in the solution increased, the tree-root structure became more robust, fewer micropores were formed, and consequently, the fluid loss was decreased.

XG can also enhance the tree-root structure by developing internal cross-linking polymer chains (Figure 15). The viscosity and the filtering property improved when the XG concentration was increased. However, XG has less influence than CMC LV on filtration properties. As discussed earlier, CMC LV has no significant role in viscosity rather than XG. Hence, the FE-SEM images should be carefully analyzed to see how the presence of CMC LV affected the microstructure of filter cakes and reduced the filtration rate.

Figure 16 shows the tree-root architecture of mud cake in the existence of GO and CMC LV. Some jellyfish shapes can be observed on the face of the mud cake shown in red circles. These individual GO plates can plug the micropores and result in a significant reduction in the filtrate volume. Water molecules are constantly present in interlayer spaces. Separate GO plates are joined together by an irregular lattice of hydrogen bonds controlled by water molecules, oxygen-containing functional groups, and other XG and CMC LV functional groups. A quantitative investigation of H-bond
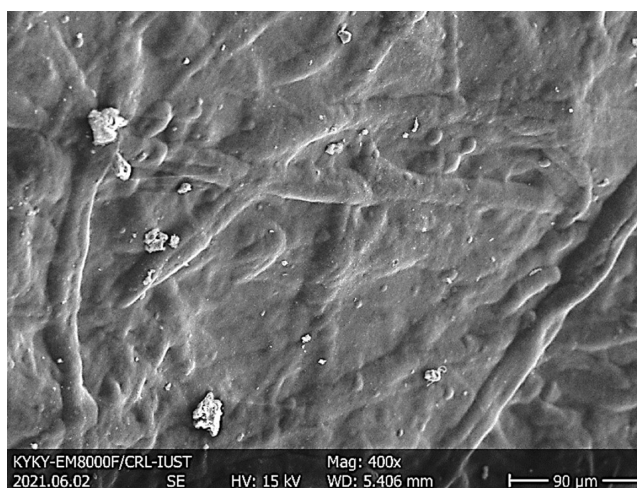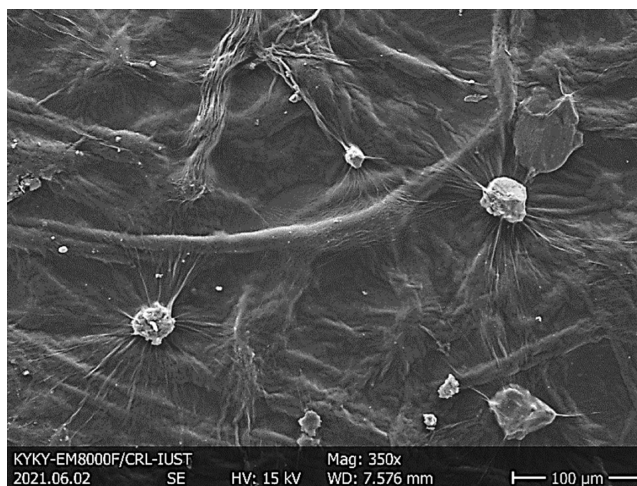

Figure 16. FE-SEM image of the dried filter cake formed by 0.15 wt % of GO and CMC LV.

network formation also reveals that these bondings are crucial in defining the overall structure of the GO-containing solutions. According to molecular dynamics studies, the features of the solutions are governed mainly by the H-bond lattice, including both functional groups in the solution and water molecules inside the interlayer space, according to molecular dynamics studies.[77]

GO plates showed a strong tendency for establishing interparticle hydrogen bonds between themselves and other particles. A smaller, stiffer particle, such as CMC LV, is better combined with GO and improved filter cake formation than XG large particles. Indeed, the GO/CMC LV combination had considerably superior filtration characteristics, and individual platelets could join together (shaped like jellyfish) and block the micropores. Consequently, whereas XG has a more significant impact on viscosity than CMC LV, CMC LV's ability to form jellyfish structures with GO platelets further reduces the filtrate volume (Figure 17).

Besides rheological and filtration performance, economic and environmental considerations play a significant role in drilling fluid selection. It is well acknowledged that reducing a drilling operation's environmental effect significantly impacts the selection of drilling fluid additives. Many of the additives
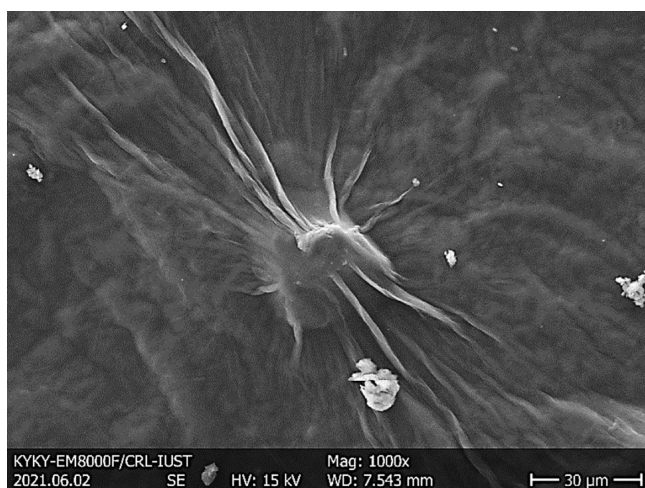
Figure 17. FE-SEM image of the jellyfish shape of individual GO on the filter cake.

used in drilling fluids are potentially hazardous. As a result, the petroleum industry's demand for minerals with high accessibility and low toxicity grows.[78] This study used GO as a high-performance additive to enhance rheological behavior and control filtration loss. GO is made from graphite, and unlike certain additives, the supply from the source is unrestricted. GO, XG, and CMC LV can be used as they are highly available and relatively inexpensive. Thus, the findings of this study can be applied to provide low-cost, stable, and environmentally compatible additives for drilling low-pressure, depleted, and fractured oil and gas reservoirs.

More study is needed to understand better the usage of GO in drilling mud in the oil and gas industry. The following are the study recommendations:

- Thorough research is necessary to conduct the interactions between graphene derivatives and other drilling fluid additives.
- Before commercialization, additional attention to cost effectiveness is required to guarantee consistency in the production of drilling fluids with better rheological characteristics.
- To create extensive techniques for the mass production of graphene derivatives, in-depth investigation is necessary.
- Drilling fluid optimization should be compared between WDFs containing GO and synthetic and oil-based drilling fluids.
- Comparison should be made with drilling fluids that have been exposed to high temperature and pressure conditions.

4. SUMMARY AND CONCLUSIONS

The effects of concentration on the rheological and filtration properties of GO/XG/CMC LV-WDF were investigated. Five different rheological models were used to understand the rheological properties better. The filtering mechanism was proposed based on viscosity and morphological studies. The following conclusions may be taken from the findings of this study:

1 The presence of GO and XG greatly enhanced the rheological characteristics of GO/CMC LV/XG-WDF.

However, the impact of CMC LV on rheological behaviors was relatively minor.

2 As GO and CMC LV concentrations increased, the API fluid loss of GO/CMC LV/XG-WDF reduced noticeably, whereas XG had less impact on the API fluid loss.

3 The Herschel–Bulkey model outperformed the other four models in forecasting the rheological parameters of GO/CMC LV/XG-WDF. The Sisko model is also acceptable for describing the rheological characteristics of GO/CMC LV/XG-WDF at some concentrations.

4 The addition of XG and CMC LV influences filter cake's microstructure, resulting in a tree-root morphology. Indeed, in the GO/CMC LV solution, the individual platelets may bind together, form a jellyfish shape, and block the micropores. Hence, CMC LV considerably affected filtration characteristics.

5 In general, GO had a substantial effect on creating a compact filter cake in the low solid GO/CMC LV/XG-WDF. At the same time, XG and CMC LV served as effective viscosifier and filtration control agents, respectively. The combination of XG and CMC LV in GO-WDF resulted in improved rheological characteristics and filtration performance.

■ AUTHOR INFORMATION

Corresponding Author

Farhad Sharif — *Department of Polymer Engineering and Color Technology, Amirkabir University of Technology, Tehran 15875-4413, Iran;* ⦿ orcid.org/0000-0002-0801-1076; Email: sharif@aut.ac.ir

Authors

Ali Rafieefar — *Department of Petroleum Engineering, Amirkabir University of Technology, Tehran 15875-4413, Iran*

Abdolnabi Hashemi — *Department of Petroleum Engineering, Petroleum University of Technology, Ahwaz 63187-14317, Iran*

Ali Mohammad Bazargan — *New Technologies Research Center (NTRC), Amirkabir University of Technology, Tehran 15875-4413, Iran*

Complete contact information is available at:
https://pubs.acs.org/10.1021/acsomega.1c04398

Notes

The authors declare no competing financial interest.

■ NOMENCLATURE

Abbreviations

GO	graphene oxide
CMC LV	low viscosity carboxymethyl cellulose
XG	xanthan gum
WDF	water-based drilling fluids
PV	plastic viscosity
AV	apparent viscosity
YP	yield point
R^2	coefficient of determination
SSR	sum of squared residuals

RSME	root mean square error
τ	shear stress
τ_0	yield stress
μ_p	plastic viscosity
μ_∞	infinite shear rate
$\dot{\gamma}$	shear rate
n	flow behavior index
K	flow consistency coefficient
API	American Petroleum Institute
rpm	rotation per minute
FE-SEM	field emission scanning electron microscopes
cP	centipoise
$NaNO_3$	sodium nitrate
H_2SO_4	sulfuric acid
$KMnO_4$	potassium permanganate
H_2O_2	hydrogen peroxide
HCl	hydrochloric acid
CH_2-COOH	carboxymethyl group
$ClCH_2-COONa$	sodium monochloroacetic acid

■ REFERENCES

(1) Li, M.-C.; Wu, Q.; Song, K.; French, A. D.; Mei, C.; Lei, T. pH-responsive water-based drilling fluids containing bentonite and chitin nanocrystals. *ACS Sustainable Chem. Eng.* **2018**, *6*, 3783−3795.

(2) Bloys, B.; Davis, N.; Smolen, B.; Bailey, L.; Houwen, O.; Reid, P.; Sherwood, J.; Fraser, L.; Hodder, M.; Montrouge, F. Designing and managing drilling fluid. *Oilfield Rev.* **1994**, *6*, 33−43.

(3) Salih, A.; Elshehabi, T.; Bilgesu, H. Impact of nanomaterials on the rheological and filtration properties of water-based drilling fluids. *SPE Eastern Regional Meeting*; Society of Petroleum Engineers, 2016.

(4) Plank, J. P.; Gossen, F. A. Visualization of fluid-loss polymers in drilling-mud filter cakes. *SPE Drill. Eng.* **1991**, *6*, 203−208.

(5) Zhou, G.; Qiu, Z.; Zhong, H.; Zhao, X.; Kong, X. Study of Environmentally Friendly Wild Jujube Pit Powder as a Water-Based Drilling Fluid Additive. *ACS Omega* **2021**, *6*, 1436−1444.

(6) Clark, P. E. Drilling mud rheology and the API recommended measurements. *SPE Production Operations Symposium*; Society of Petroleum Engineers, 1995.

(7) Bageri, B. S.; Gamal, H.; Elkatatny, S.; Patil, S. Effect of Different Weighting Agents on Drilling Fluids and Filter Cake Properties in Sandstone Formations. *ACS Omega* **2021**, *6*, 16176.

(8) Hashemizadeh, A.; Maaref, A.; Shateri, M.; Larestani, A.; Hemmati-Sarapardeh, A. Experimental measurement and modeling of water-based drilling mud density using adaptive boosting decision tree, support vector machine, and K-nearest neighbors: A case study from the South Pars gas field. *J. Pet. Sci. Eng.* **2021**, *207*, 109132.

(9) Sensoy, T.; Chenevert, M. E.; Sharma, M. M. Minimizing water invasion in shales using nanoparticles. *SPE Annual Technical Conference and Exhibition*; Society of Petroleum Engineers: 2009.

(10) Tian, Y.; Liu, X.; Luo, P.; Huang, J.; Xiong, J.; Liang, L.; Li, W. Study of a Polyamine Inhibitor Used for Shale Water-Based Drilling Fluid. *ACS Omega* **2021**, *6*, 15448.

(11) Warren, B.; van der Horst, P.; Stewart, W. Application of amphoteric cellulose ethers in drilling fluids, *International Symposium on Oilfield Chemistry*; Society of Petroleum Engineers, 2003.

(12) Iscan, A. G.; Kok, M. V. Effects of polymers and CMC concentration on rheological and fluid loss parameters of water-based drilling fluids. *Energy Sources, Part A* **2007**, *29*, 939−949.

(13) Dias, F. T. G.; Souza, R. R.; Lucas, E. F. Influence of modified starches composition on their performance as fluid loss additives in invert-emulsion drilling fluids. *Fuel* **2015**, *140*, 711−716.

(14) Li, M.-C.; Wu, Q.; Song, K.; Lee, S.; Jin, C.; Ren, S.; Lei, T. Soy protein isolate as fluid loss additive in bentonite−water-based drilling fluids. *ACS Appl. Mater. Interfaces* **2015**, *7*, 24799−24809.

(15) Yan, L.; Wang, C.; Xu, B.; Sun, J.; Yue, W.; Yang, Z. Preparation of a novel amphiphilic comb-like terpolymer as viscosifying additive in low-solid drilling fluid. *Mater. Lett.* **2013**, *105*, 232−235.

(16) Nunes, R. d. C. P.; Pires, R. V.; Lucas, E. F.; Vianna, A.; Lomba, R. New filtrate loss controller based on poly (methyl methacrylate-co-vinyl acetate). *J. Appl. Polym. Sci.* **2014**, *131*, 40646.

(17) Ma, J.; Xia, B.; Yu, P.; An, Y. Comparison of an Emulsion-and Solution-Prepared Acrylamide/AMPS Copolymer for a Fluid Loss Agent in Drilling Fluid. *ACS Omega* **2020**, *5*, 12892−12904.

(18) Magzoub, M. I.; Salehi, S.; Hussein, I. A.; Nasser, M. S. Investigation of Filter Cake Evolution in Carbonate Formation Using Polymer-Based Drilling Fluid. *ACS Omega* **2021**, *6*, 6231−6239.

(19) Jung, Y.; Son, Y.-H.; Lee, J.-K.; Phuoc, T. X.; Soong, Y.; Chyu, M. K. Rheological behavior of clay−nanoparticle hybrid-added bentonite suspensions: specific role of hybrid additives on the gelation of clay-based fluids. *ACS Appl. Mater. Interfaces* **2011**, *3*, 3515−3522.

(20) Cai, J.; Chenevert, M. E. E.; Sharma, M. M. M.; Friedheim, J. Decreasing water invasion into Atoka shale using nonmodified silica nanoparticles. *SPE Drill. Completion* **2012**, *27*, 103−112.

(21) Kosynkin, D. V.; Ceriotti, G.; Wilson, K. C.; Lomeda, J. R.; Scorsone, J. T.; Patel, A. D.; Friedheim, J. E.; Tour, J. M. Graphene oxide as a high-performance fluid-loss-control additive in water-based drilling fluids. *ACS Appl. Mater. Interfaces* **2012**, *4*, 222−227.

(22) Fazelabdolabadi, B.; Khodadadi, A. A.; Sedaghatzadeh, M. Thermal and rheological properties improvement of drilling fluids using functionalized carbon nanotubes. *Appl. Nanosci.* **2015**, *5*, 651−659.

(23) Zamir, A.; Siddiqui, N. Investigating and enhancing mud cake reduction using smart nano clay based WBM. *J. Pet. Environ. Biotechnol.* **2017**, *8*, 315.

(24) Moghadasi, R.; Rostami, A.; Hemmati-Sarapardeh, A.; Motie, M. Application of Nanosilica for inhibition of fines migration during low salinity water injection: Experimental study, mechanistic understanding, and model development. *Fuel* **2019**, *242*, 846−862.

(25) Mcelfresh, P. M.; Wood, M.; Ector, D. Stabilizing nano particle dispersions in high salinity, high temperature downhole environments. *SPE International Oilfield Nanotechnology Conference and Exhibition*; Society of Petroleum Engineers, 2012.

(26) Hemmati-Sarapardeh, A.; Varamesh, A.; Husein, M. M.; Karan, K. On the evaluation of the viscosity of nanofluid systems: Modeling and data assessment. *Renewable Sustainable Energy Rev.* **2018**, *81*, 313−329.

(27) Vryzas, Z.; Mahmoud, O.; Nasr-El-Din, H. A.; Kelessidis, V. C. Development and testing of novel drilling fluids using Fe 2 O 3 and SiO 2 nanoparticles for enhanced drilling operations. *International Petroleum Technology Conference*; International Petroleum Technology Conference, 2015.

(28) Mahmoud, O.; Nasr-El-Din, H. A.; Vryzas, Z.; Kelessidis, V. C. Using ferric oxide and silica nanoparticles to develop modified calcium bentonite drilling fluids. *SPE Drill. Completion* **2018**, *33*, 12−26.

(29) Ghasemi, M.; Moslemizadeh, A.; Shahbazi, K.; Mohammadzadeh, O.; Zendehboudi, S.; Jafari, S. Primary evaluation of a natural surfactant for inhibiting clay swelling. *J. Pet. Sci. Eng.* **2019**, *178*, 878−891.

(30) Singh, S. K.; Ahmed, R. M.; Growcock, F. Vital role of nanopolymers in drilling and stimulations fluid applications. *SPE Annual Technical Conference and Exhibition*; Society of Petroleum Engineers, 2010.

(31) Pham, H.; Nguyen, Q. P. Effect of silica nanoparticles on clay swelling and aqueous stability of nanoparticle dispersions. *J. Nanopart. Res.* **2014**, *16*, 2137.

(32) Contreras, O.; Hareland, G.; Husein, M.; Nygaard, R.; Al-saba, M. T. Experimental investigation on wellbore strengthening in shales by means of nanoparticle-based drilling fluids. *SPE Annual Technical Conference and Exhibition*; Society of Petroleum Engineers, 2014.

(33) Abu-Jdayil, B.; Ghannam, M. The modification of rheological properties of sodium bentonite-water dispersions with low viscosity CMC polymer effect. *Energy Sources, Part A* **2014**, *36*, 1037−1048.

(34) Divandari, H.; Hemmati-Sarapardeh, A.; Schaffie, M.; Husein, M. M.; Ranjbar, M. Conformance Control in Oil Reservoirs by Citric Acid-Coated Magnetite Nanoparticles. *ACS Omega* **2021**, *6*, 9001−9012.

(35) Hoelscher, K. P.; Young, S.; Friedheim, J.; De Stefano, G. Nanotechnology application in drilling fluids. *Offshore Mediterranean Conference and Exhibition*; Offshore Mediterranean Conference, 2013.

(36) William, J. K. M.; Ponmani, S.; Samuel, R.; Nagarajan, R.; Sangwai, J. S. Effect of CuO and ZnO nanofluids in xanthan gum on thermal, electrical and high pressure rheology of water-based drilling fluids. *J. Pet. Sci. Eng.* **2014**, *117*, 15−27.

(37) Srivatsa, J. T.; Ziaja, M. B. An experimental investigation on use of nanoparticles as fluid loss additives in a surfactant−polymer based drilling fluid. *IPTC 2012: International Petroleum Technology Conference*; European Association of Geoscientists & Engineers, 2012; pp280.

(38) Fakoya, M.; Shah, S. Enhancement of filtration properties in surfactant-based and polymeric fluids by nanoparticles. *SPE Eastern Regional Meeting*; Society of Petroleum Engineers, 2014.

(39) Corredor-Rojas, L. M.; Hemmati-Sarapardeh, A.; Husein, M. M.; Dong, M.; Maini, B. B. Rheological behavior of surface modified silica nanoparticles dispersed in partially hydrolyzed polyacrylamide and xanthan gum solutions: Experimental measurements, mechanistic understanding, and model development. *Energy Fuels* **2018**, *32*, 10628−10638.

(40) Saboori, R.; Sabbaghi, S.; Mowla, D.; Soltani, A. Decreasing of water loss and mud cake thickness by CMC nanoparticles in mud drilling. *Int. J. Nano Dimens.* **2012**, *3*, 101−104.

(41) Li, G.; Zhang, J.; Hou, Y. Nanotechnology to improve sealing ability of drilling fluids for shale with micro-cracks during drilling. *SPE International Oilfield Nanotechnology Conference and Exhibition*; Society of Petroleum Engineers, 2012.

(42) Quintero, L.; Cardenas, A. E.; Clark, D. E. Nanofluids and methods of use for drilling and completion fluids. U.S. Patent, 20,120,015,852 A1, 2014.

(43) Gudarzifar, H.; Sabbaghi, S.; Rezvani, A.; Saboori, R. Experimental investigation of rheological & filtration properties and thermal conductivity of water-based drilling fluid enhanced. *Powder Technol.* **2020**, *368*, 323−341.

(44) Taha, N. M.; Lee, S. Nano graphene application improving drilling fluids performance. *International Petroleum Technology Conference*; International Petroleum Technology Conference, 2015.

(45) Caenn, R.; Darley, H. C.; Gray, G. R. *Composition and Properties of Drilling and Completion Fluids*; Gulf professional publishing, 2011.

(46) Santos, N. B. C.; Fagundes, F. M.; de Oliveira Arouca, F.; Damasceno, J. J. R. Sedimentation of solids in drilling fluids used in oil well drilling operations. *J. Pet. Sci. Eng.* **2018**, *162*, 137−142.

(47) Balandin, A. A.; Ghosh, S.; Bao, W.; Calizo, I.; Teweldebrhan, D.; Miao, F.; Lau, C. N. Superior thermal conductivity of single-layer graphene. *Nano Lett.* **2008**, *8*, 902−907.

(48) Nasrollahzadeh, M.; Babaei, F.; Fakhri, P.; Jaleh, B. Synthesis, characterization, structural, optical properties and catalytic activity of reduced graphene oxide/copper nanocomposites. *RSC Adv.* **2015**, *5*, 10782−10789.

(49) Barel, A. O.; Paye, M.; Maibach, H. I. *Handbook of Cosmetic Science and Technology*; CRC Press, 2014.

(50) Kukrety, A.; Singh, R. K.; Singh, P.; Ray, S. S. Comprehension on the synthesis of carboxymethylcellulose (CMC) utilizing various cellulose rich waste biomass resources. *Waste Biomass Valorization* **2018**, *9*, 1587−1595.

(51) Gudarzi, M. M.; Sharif, F. Self assembly of graphene oxide at the liquid−liquid interface: A new route to the fabrication of graphene based composites. *Soft Matter* **2011**, *7*, 3432−3440.

(52) Yousefi, N.; Gudarzi, M. M.; Zheng, Q.; Aboutalebi, S. H.; Sharif, F.; Kim, J.-K. Self-alignment and high electrical conductivity of ultralarge graphene oxide−polyurethane nanocomposites. *J. Mater. Chem.* **2012**, *22*, 12709−12717.

(53) Bazargan, A. M.; Sharif, F.; Mazinani, S.; Naderi, N. Highly conductive reduced graphene oxide transparent ultrathin film through joule-heat induced direct reduction. *J. Mater. Sci.: Mater. Electron.* **2017**, *28*, 1419−1427.

(54) Yousefi, N.; Gudarzi, M. M.; Zheng, Q.; Lin, X.; Shen, X.; Jia, J.; Sharif, F.; Kim, J.-K. Highly aligned, ultralarge-size reduced graphene oxide/polyurethane nanocomposites: mechanical properties and moisture permeability. *Composites, Part A* **2013**, *49*, 42−50.

(55) Mianehrow, H.; Moghadam, M. H.; Sharif, F.; Mazinani, S. Graphene-oxide stabilization in electrolyte solutions using hydroxyethyl cellulose for drug delivery application. *Int. J. Pharm.* **2015**, *484*, 276−282.

(56) Katzbauer, B. Properties and applications of xanthan gum. *Polym. Degrad. Stab.* **1998**, *59*, 81−84.

(57) Viebke, C.; Williams, P. Determination of molecular mass distribution of κ-carrageenan and xanthan using asymmetrical flow field-flow fractionation. *Food Hydrocolloids* **2000**, *14*, 265−270.

(58) Houwen, O. H. Chemical characterization of CMC and its relationship to drilling-mud rheology and fluid loss. *SPE Drill. Completion* **1993**, *8*, 157−164.

(59) API, RP, 13B-1. *Recommended Practice Standard for Field Testing Water-Based Drilling Fluids*, 2003.

(60) Ziaee, H.; Arabloo, M.; Ghazanfari, M. H.; Rashtchian, D. Herschel−Bulkley rheological parameters of lightweight colloidal gas aphron (CGA) based fluids. *Chem. Eng. Res. Des.* **2015**, *93*, 21−29.

(61) Sisko, A. W. The flow of lubricating greases. *Ind. Eng. Chem. Res.* **1958**, *50*, 1789−1792.

(62) Dhiman, A. S. Rheological properties & corrosion characteristics of drilling mud additives. M. Sc thesis, Dalhouse University, 2012.

(63) Amani, M.; Hassiba, K. J. Salinity effect on the rheological properties of water based mud under high pressures and high temperatures of deep wells. *SPE Kuwait International Petroleum Conference and Exhibition*; Society of Petroleum Engineers, 2012.

(64) Quan, H.; Li, H.; Huang, Z.; Zhang, T.; Dai, S. Copolymer SJ-1 as a fluid loss additive for drilling fluid with high content of salt and calcium. *Int. J. Polym. Sci.* **2014**, *2014*, 201301.

(65) Benyounes, K.; Mellak, A.; Benchabane, A. The effect of carboxymethylcellulose and xanthan on the rheology of bentonite suspensions. *Energy Sources, Part A* **2010**, *32*, 1634−1643.

(66) Park, S.; Lee, K.-S.; Bozoklu, G.; Cai, W.; Nguyen, S. T.; Ruoff, R. S. Graphene oxide papers modified by divalent ions—enhancing mechanical properties via chemical cross-linking. *ACS Nano* **2008**, *2*, 572−578.

(67) Ikram, R.; Mohamed Jan, B.; Sidek, A.; Kenanakis, G. Utilization of Eco-Friendly Waste Generated Nanomaterials in Water-Based Drilling Fluids; State of the Art Review. *Materials* **2021**, *14*, 4171.

(68) Ma, J.; Yu, P.; Xia, B.; An, Y. Micro-manganese as a weight agent for improving the suspension capability of drilling fluid and the study of its mechanism. *RSC Adv.* **2019**, *9*, 35509−35523.

(69) Bridges, S.; Robinson, L. *A Practical Handbook for Drilling Fluids Processing*; Gulf Professional Publishing, 2020.

(70) Hafshejani, K. S.; Moslemizadeh, A.; Shahbazi, K. A novel bio-based deflocculant for bentonite drilling mud. *Appl. Clay Sci.* **2016**, *127−128*, 23−34.

(71) Li, W.; Zhao, X.; Ji, Y.; Peng, H.; Chen, B.; Liu, L.; Han, X. Investigation of biodiesel-based drilling fluid, part 1: biodiesel evaluation, invert-emulsion properties, and development of a novel emulsifier package. *SPE J.* **2016**, *21*, 1755−1766.

(72) Lyons, W. *Working Guide to Drilling Equipment and Operations*; Gulf Professional Publishing, 2009.

(73) Nwosu, O.; Ewulonu, C. Rheological behaviour of eco-friendly drilling fluids from biopolymers. *J. Polym. Biopolym. Phys. Chem.* **2014**, *2*, 50−54.

(74) Blkoor, S.; Fattah, K. The influence of XC-polymer on drilling fluid filter cake properties and formation damage. *J. Pet. Environ. Biotechnol.* **2013**, *4*, 157.

(75) API SPEC 13A (1993). *Specification for Drilling Fluid Materials*; American Petroleum Institute, 1993.

(76) Bülichen, D.; Plank, J. Role of colloidal polymer associates for the effectiveness of hydroxyethyl cellulose as a fluid loss control additive in oil well cement. *J. Appl. Polym. Sci.* **2012**, *126*, E25−E34.

(77) Medhekar, N. V.; Ramasubramaniam, A.; Ruoff, R. S.; Shenoy, V. B. Hydrogen bond networks in graphene oxide composite paper: structure and mechanical properties. *ACS Nano* **2010**, *4*, 2300−2306.

(78) Moslemizadeh, A.; Khezerloo-ye Aghdam, S.; Shahbazi, K.; Zendehboudi, S. A triterpenoid saponin as an environmental friendly and biodegradable clay swelling inhibitor. *J. Mol. Liq.* **2017**, *247*, 269−280.